CLIO report

Khodnevych Vitalii, Nicolas Delerue

August 22, 2017

Contents

We report on measurements of Coherent Smith-Purcell radiation at the CLIO Free Electron Laser. Smith-Purcell radiation is emitted when a grating is brought close from a bunch of relativistic particles. When the bunch is sufficiently short coherent radiation is emitted. This coherent radiation encodes the longitudinal form factor of the bunch and can therefore be used as a longitudinal profile monitor.

1 Brief theory of Smith-Purcell radiation

Smith-Purcell radiation (SPR) occurs when a charged particle move above a metallic periodic structure. Emitted radiation is spread in solid angle. The wavelength of the radiation for SPR depends on the observation angle Θ according to the following formula:

$$\lambda = \frac{l}{n}(\frac{1}{\beta} - cos\Theta) \tag{1}$$

where l is the grating period , n is the order of radiation, Θ is the observation angle and β is the relativistic velocity.

For one electron the emission spectrum (single electron yield [1]) is given by:

$$\frac{d^2I_1}{d\omega d\Omega} = \frac{e^2\omega^2 l^2}{4\pi^2 c^3} R^2 exp(-2x_0/\lambda_e) \tag{2}$$

where ω is the emission frequency, $d\Omega$ is the solid angle, e is the electron charge, c is the speed of light, R^2 is the "grating efficiency factor", x_0 is the beam-grating separation (BGS) and λ_e is the evanescent wavelength:

$$\lambda_e = \lambda \frac{\beta\gamma}{2\pi\sqrt{1 + (\beta\gamma \sin\Theta \sin\phi)^2}} \tag{3}$$

where β, γ are the relativistic parameters of the particles in the beam. The total spectrum is proportional to the single electron yield and contains incoherent and coherent components:

$$\frac{d^2I}{d\omega d\Theta} = \frac{d^2I_1}{d\omega d\Theta}[N + N(N-1)F(\omega)] \tag{4}$$

Where N is the number of electrons in the bunch and $F(\omega)$ is the form factor of the time profile of the bunch. Using the phase recovery methods, such as Kramers-Kronig or Hilbert [2], it is possible to recover the phase and then the time profile of the bunch.

So Smith-Purcell radiation can be used to monitor the longitudinal beam profile.

2 CLIO

The CLIO free electron laser is an accelerator built in 1991. It is described in details in [**?**] and it is shown on figure 1. The CLIO accelerator consist of a thermionic

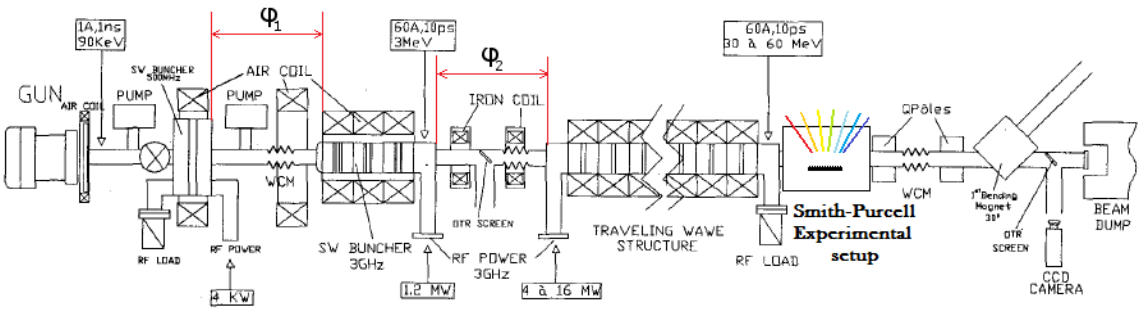

Figure 1: Layout of the CLIO accelerator and position of the experimental setup: $\varphi_1 = \phi_B$, $\varphi_2 = \phi_S$.

gun, a subharmonic buncher (SHB), a fundamental buncher (FB) and an accelerating cavity (AC). The gun produce bunches about 1.5 ns long at an energy of 90 keV. These bunch are then compressed by the subharmonic buncher to 200 ps or less to make it suitable for further compression with the fundamental buncher. This fundamental buncher further compresses the beam to a few ps and accelerates bunch to several MeV, making the electrons relativistic. The bunches are then further accelerated in the accelerating cavity to the operation energy (typically 10-45 MeV).

For bunch compression the most important parameters are the phases φ_1 (between SHB and FB), φ_2 (between FB and AC) and power of FB.

3 Experimental setup

The experimental setup is shown on figure 2. It consist of 12 pyrodetectors placed from 48^o to 125^o with 7^o separation. To collect the emitted radiation 25 mm diameter off-axis parabolic mirrors are used. The signal from the detectors is amplified and then digitized by a data 12 bits 1 MS/s acquisition system.

The experiment uses a 40x20 mm aluminium grating with 3 mm pitch. The beam-grating separation can be changed by a stepper motor.

3.1 Data Acquisition

Data is taken with DAQ board with 250 ksps sampling rate. Python script (read_plot_data.py) Analyze single file with taken data and produce the the array of signals on chosen channels. Noise filtering is implemented inside script. We use simple FFT filtering by turning in zero high frequency component of modulus of FT of the signal. Depth of filtering could be chosen by user. Signal is extracting from filtered data

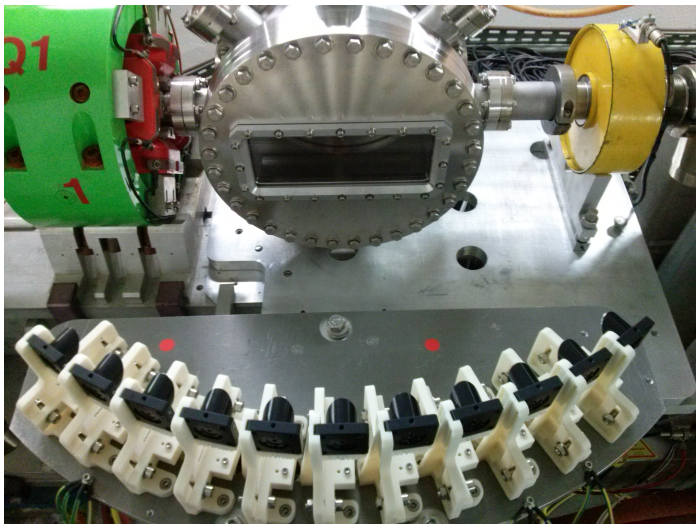

Figure 2: Experimental setup for SPR measurements at CLIO: set of twelve pyrodectors with off axis parabolic mirrors placed equidistantly with 7^o separation and experimental chamber with the grating inside.

on falling edge of electron signal and computed as difference of signal amplitude at equidistant positions from the edge. This give amplitude on detector when bunch pass grating and with respect to the moment before. Except this electron signal amplitude is acquired as simple min. For this type of the signal we remove constant component with FFT and live other components as they are. After script finish his work, .sig file is generated. In this file, except spectral component and electron signal, we also have some additional information like position of the grating, time and date, etc. After measurements, .sig files are collected and analyzed with matlab.

Other option is online analysis with Spectrum analyzing tool (see fig. 3). Its allow to monitor in online regime position of data taken, spectrum and Form factor. It has option of choose of time period, position of spectrum, energy and beam-grating separation for Form factor recovering.

4 Data processing and analysis

In current experimental setup we could change only beam-grating separation (BGS). SPR exponentially increase with decrease of BGS. Fit of this dependence will give value of evanescent wave and will help to estimate level of background.

At the first stage of our analysis we will try to proof presence of SPR and will try check basic properties of it.

At second stage will try to extract data from this spectrums and compare with simulation.

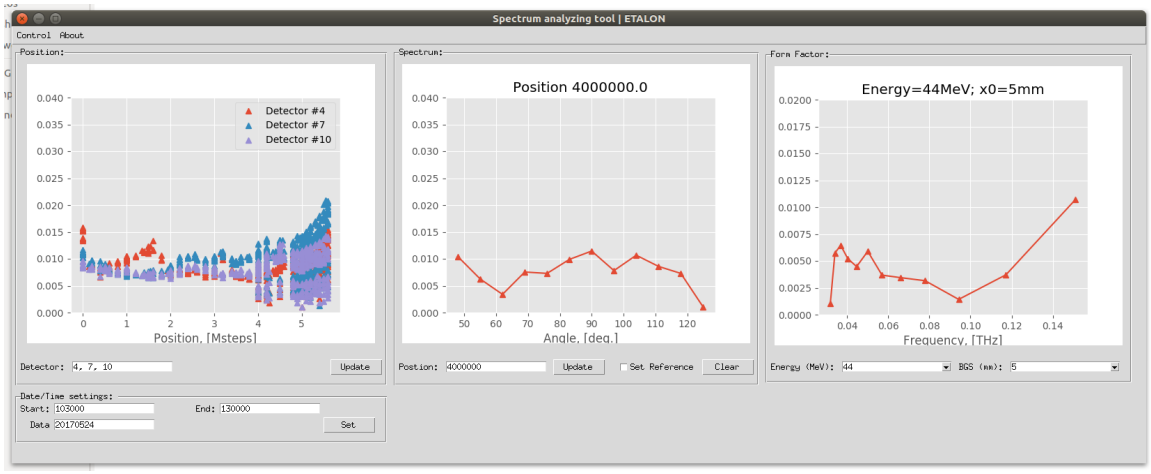

Figure 3: Spectrum analyzing tool GUI.

4.1 Data analysis

As sampling rate is high (250 ksps) and accelerator repetition rate is low (25 Hz), usually in one file we have one signal or no signal at all, but this file anyway was processed. So at the analysis stage we reject data with zero electron intensity by applying the cut in analyzing code. Also we cut events with incorrect measured amplitude by cutting single high-amplitude events on 12 channel, as this channel didn't see signal and only noise. All the data normalized by electron signal intensity.

4.1.1 Smith-Purcell theory prediction

According to Smith-Purcell theory, we expect to see exponential decay of the signal as function of beam-grating separation (see fig.4) Close to the beam, signal reach

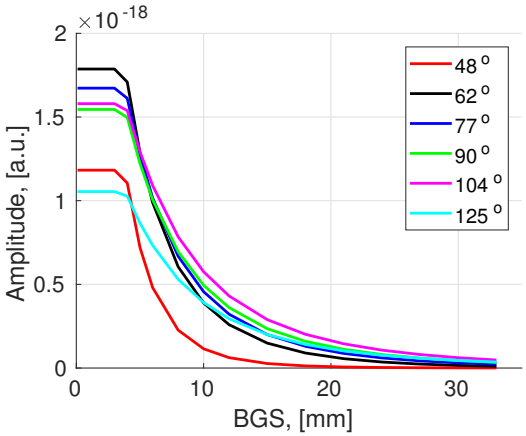

Figure 4: Decay of SPR signal as function of BGS (gfw calculation). In calculation was used CLIO beam parameters for 3mm grating

saturation, as it touch the beam.

4.1.2 Experimental results

We made wide scan of amplitudes for different beam-grating separation. But instead of clear exponent we see in figure 5 complicate curve. Result is reproducible for two different buncher phases. For different angles shape of the curve is different, but all of them have exponential increase close to beam (or linear in log scale). So further measurements will be done in this narrow region near the beam.

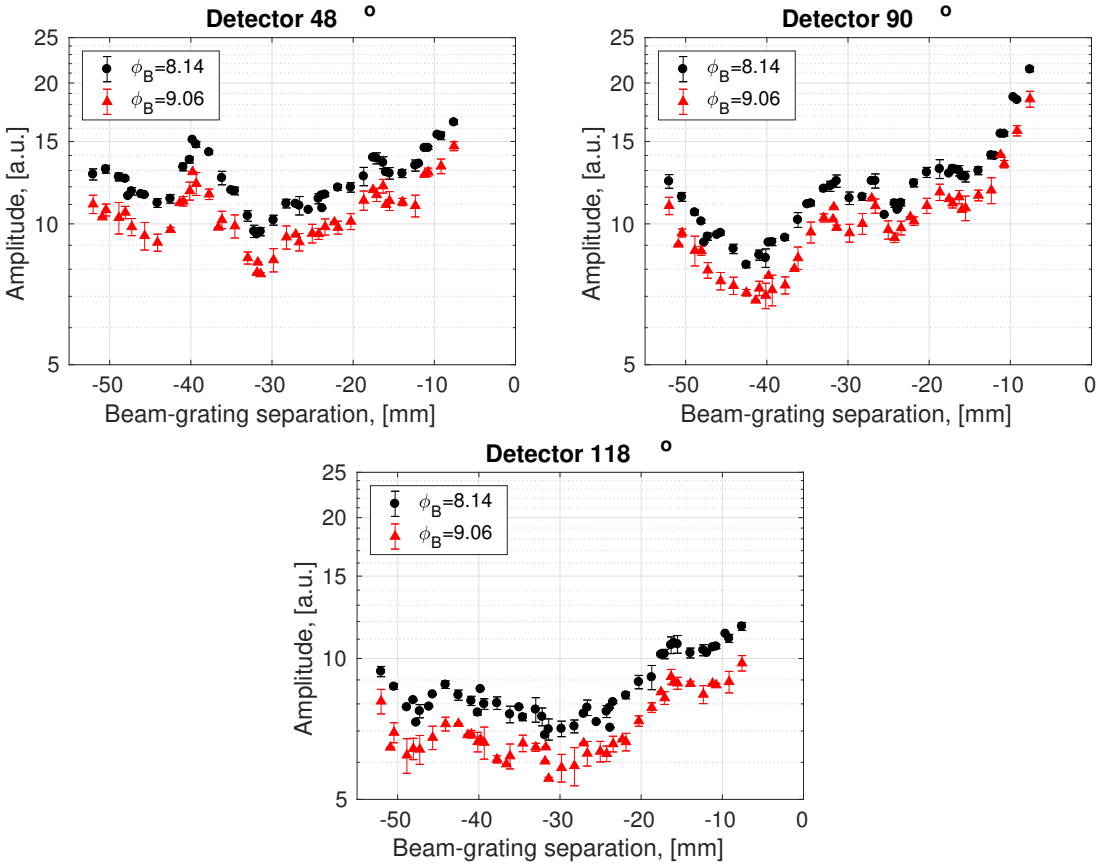

Figure 5: Amplitude as function of BGS (Wide scan). Pattern far from the beam is under investigation. 6 mm grating, "good" beam.

Its clear seen from figures 5, that except SP signal in total signal present also background, which have non random behavior, as we could also see from figures 6. With approaching to the beam, we saw increase of the signal is probably SP radiation. At region far from the beam, we see some pattern, nature of which should be investigated.

In log scale we could see in figure 7 two signal components: SPR signal (we suppose) and background.

As we could see, we could measure signal only in small region near beam, which in real life could impact on beam. So background rejection technique's should be applied (THz mesh or WAP filters).

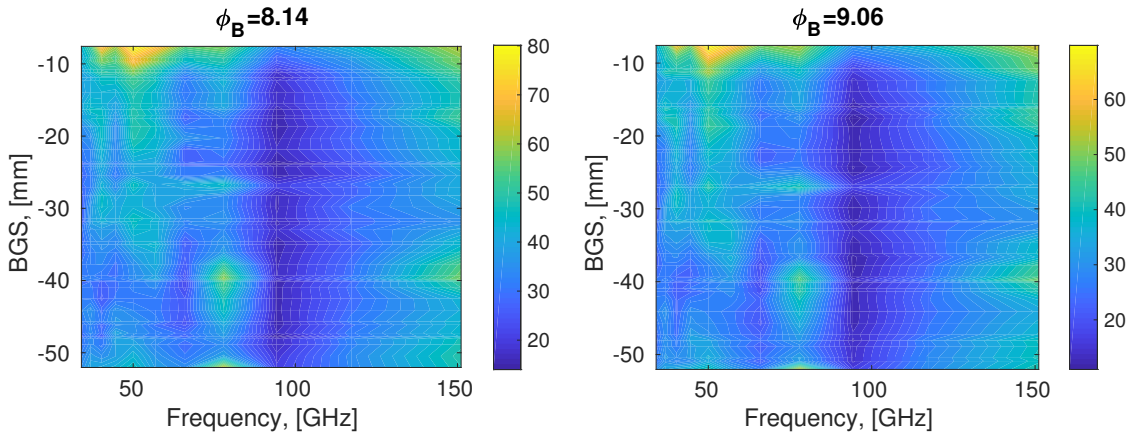

Figure 6: Background pattern as function of BGS for different buncher phases. Frequency was calculated for current grating (6 mm) as function of observation angle.

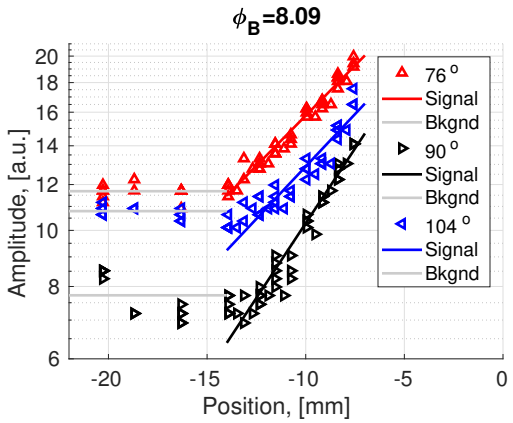

Figure 7: Signal and background with fits for different observation angles.

We divide signal in region of break by two subregions: background (fitted by grey lines) and signal (color lines). We assume that in this narrow region background is constant, so we fit data from -Inf (approx 20 mm) to intercept of two "lines" (background and signal). This give us background level. Then we choose data points, which are higher than this level and fit them by exponent. This method allow us get better fit, when signal level is low.

In result we have three coefficients: background, amplitude of the signal and decay wavelength.

During first part of our experiment we change buncher phase ϕ_B of the accelerator. Of course this also change the the electron beam intensity as shown on figure 8a. **Each time signal was normalized by this value.**

As we see on figure 8b value of background is also changing as function of phase. This could indicate two thing: background is phase dependent or current method gives bad signal extraction. Of course, its not all possibilities and this phenomena should be investigated. Reader should also take into account, that signal, which is

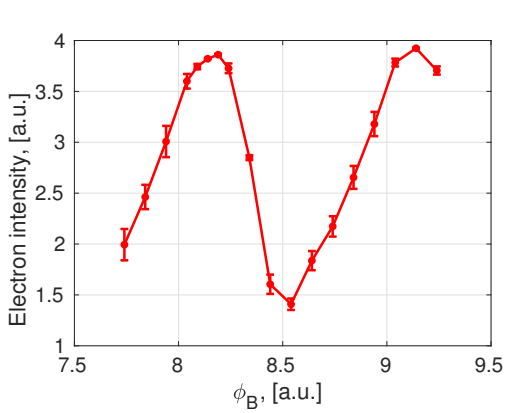

(a) Electron signal amplitude as function of buncher phase.

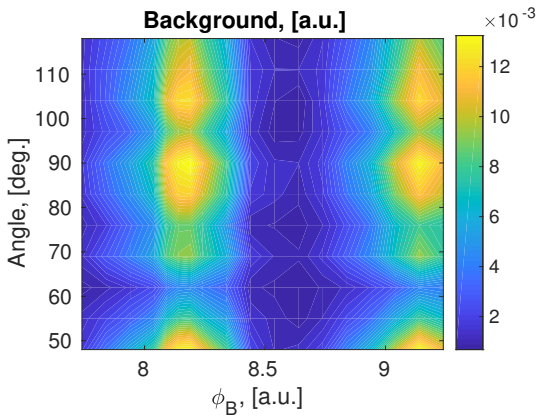

(b) Background map, obtained from fit results.

Figure 8: Experimental results

used to fit the background was normalized by electron signal.

As was mentioned above, decay length of SP signal if angle-dependent and could be used as indicator of SPR from side and test-check of alignment from other side. We find that with "good bunch" (see fig. 9), decay wavelength is stable and phase independent, as it should be. When the signal is low, we have bad fit and distorted result. This guess could be proofed by R^2 map of goodness of fit (see fig. 10). Its could be also caused by change of gamma factor (energy of bunch is changing with buncher phase). From other side, this could indicate on other effect, which is measured by our system too.

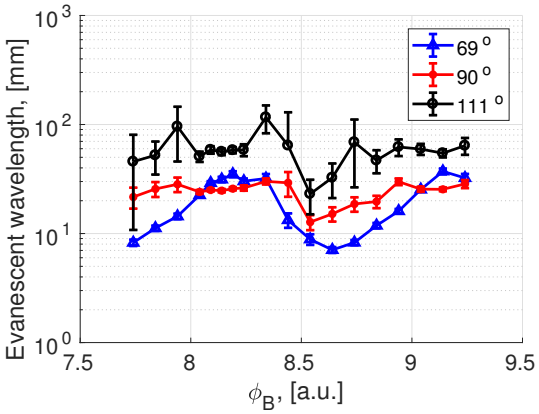

(a) Some angles

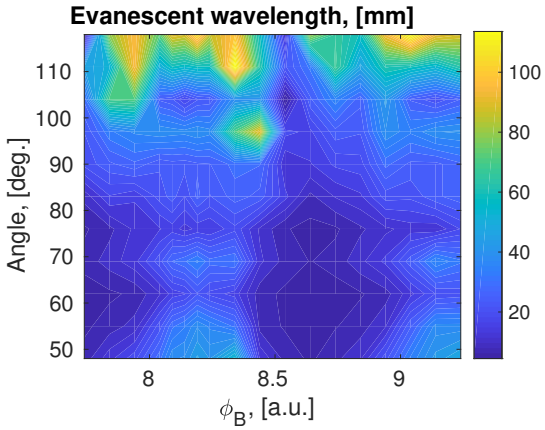

(b) All angles

Figure 9: Change of evanescent wavelength as function of buncher phase

We take weighted mean and compare evanescent wavelength with predicted by the theory of SPR. From figure 11 we see total tilt of 2 degrees. Measurements at

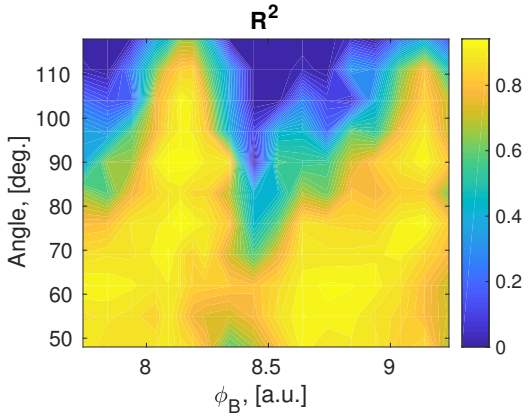

Figure 10: Goodness of fit. Some of the measured data with bad quality of beam or specific channel have noisy data and bad fit in result. R^2 was used to make cut on data and correctly evaluate evanescent wavelength

other day (19/07) confirm our assumption. At this day detector mount height was increased by 1 cm, while individual decettor alignment was kept constant. General pattern of evanescent wave distribution was saved and moved up. So in this was, we decrease tilt by 1 degree.

Particularly it could also be caused by misalignment of the optical system. Because of long measured wavelengthes, focal spot is also big, so input aperture of the OAP mirror is bigger. This correction was described in appendix and was used to extract form factor from data.

Decay length at 48^o is bigger that predicted, so in this signal component could impact also other effect. Measurements at 19/07 confirm this trend.

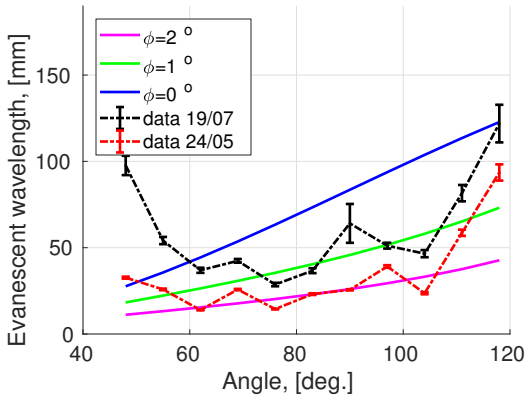

Figure 11: Evanescent wavelength as function of angle. Black is experimental data, coulour is prediction for current grating with current γ. ϕ angle is azimuthal angle and Angle on X axis is polar angle.

Amplitude plots on figure 12 present spectrum at 0 beam-grating separation. We

see that is changing with buncher phase. Angular components changing independently, contrary to background change, so we could assume, that it was caused by coherent phenomenas and we could hope that we could see also bunch shape change. Detail investigation of spectrum and Form Factor at different beam-grating separation will be done later.

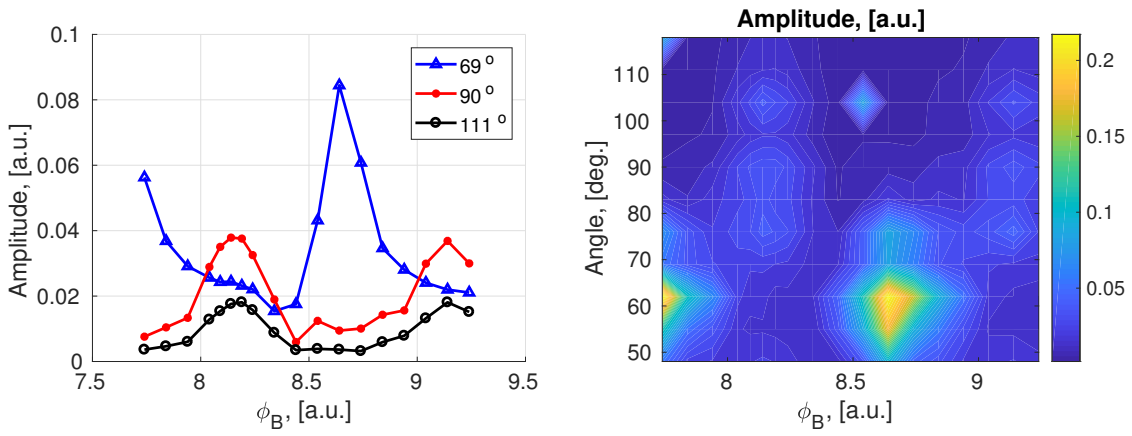

(a) 1D for different angles

(b) 2D map in phase-angle space

Figure 12: Amplitude of exponent from fit results

4.1.3 Amplitude correlation

One of the important question is relative change of frequency components in the spectrum. If all components are changing same, so that mean that it could be caused by background and not by SPR. On figure 12 we could see simultaneous increase of amplitude at some angles and decrease at others. To discover this plot correlation map of signal at region with "good bunch" (see fig. 13a). At this figure we see two correlation islands. Biggest one (at big angles) belongs to SP effect and define limit frequency of Form factor.

Correlation give general idea of dependence of spectral components. From other side we want to saw general trend in our data. For this we choose signal at 90^o as reference and plot all other one as function of it (see fig. 13b). On this plot we see two regions, which correspond to "good" and "bad" beam. "Good" beam have bigger intensity of the signal ($\sim Q^2$) than "bad". Gap between two data set correspond to fast change of bunch properties as function of buncher phase.

We notice that in region of "good" beam data have linear dependence with respect to 90^o signal. We fit this data with linear function and plot results on fig. 14. Slope as function of angle (see fig. 14a) has follow behavior: increase of signal at 90^o cause increase signal at other, high angles, and don't cause at small one. As during buncher phase manipulation we mostly change Form factor, so this plot 14a show limits in which form factor is changing. With base of the fit (see fig. 14b) situation is follow: when signal on 90^o is zero, so form factor is very thin and signal on other high angles

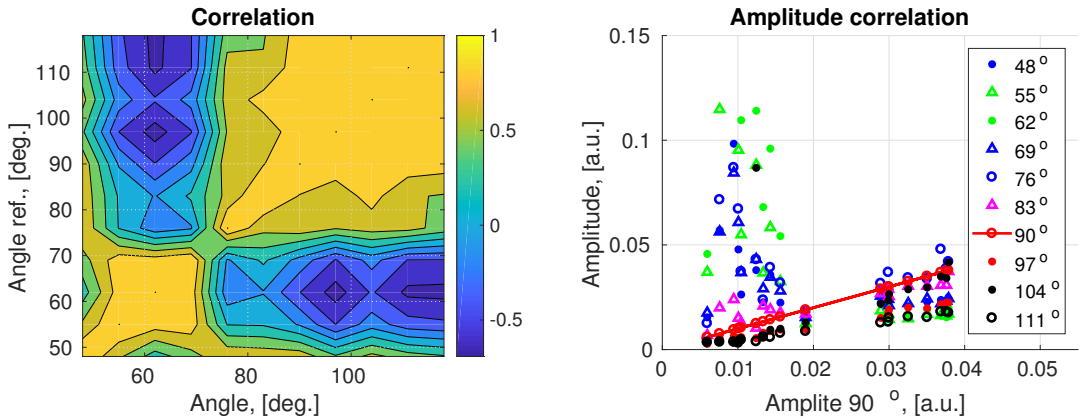

(a) Correlation map of amplitude at different angles

(b) Amplitude of signal at different angles as function of 90^o signal.

Figure 13: Amplitude correlation

also zero. But at low angles rest incoherent part, distribution of which mostly defined by SEY.

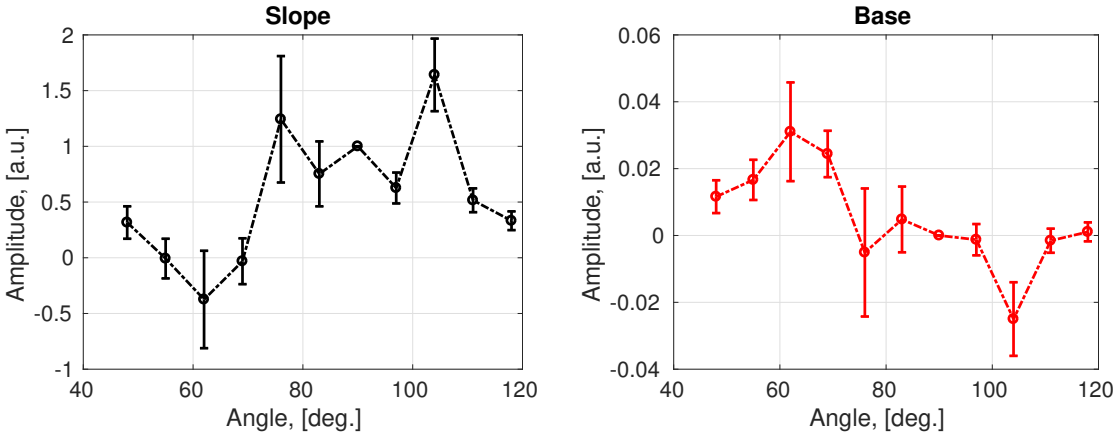

(a) Slope of the fit with 90^o reference

(b) Base of the fit with 90^o reference

Figure 14: Amplitude correlation

To be honest in our analysis, we take as reference signal on other angles too. Result of it is presented on fig. 15a and fig. 15b. Conclusion is same.

4.2 Spectrum analysis

Using fitting results, we could more precisely reconstruct spectrum and reject background. Using GFW code and experimental setup correction, we could calculate single electron yield and predicted spectrum for certain bunch length and shape. In figure 16a is shown measured spectrum for buncher phase equal $\phi_B = 8.14$ and three

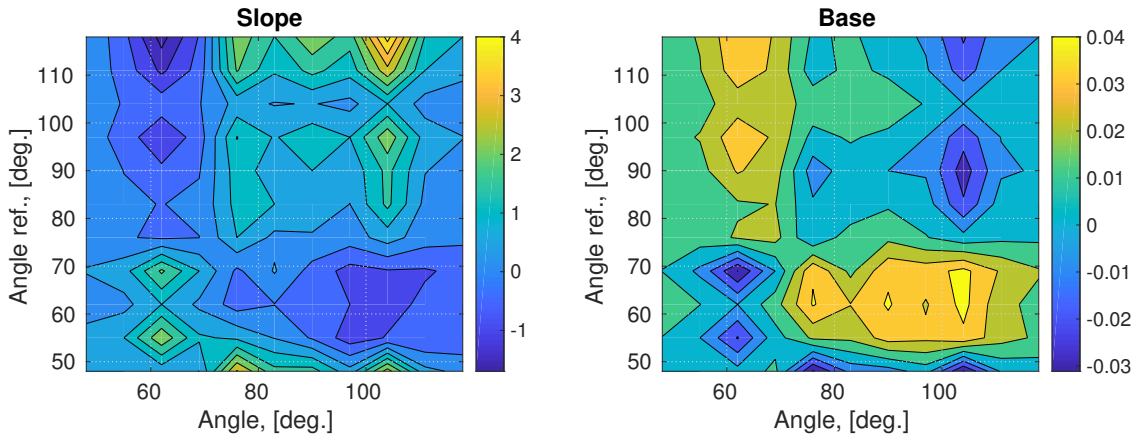

(a) Slope of the fit

(b) Base of the fit

Figure 15: Amplitude correlation

spectrums for gaussian beam and different bunch duration. By width the most suitable is 5ps gaussian bunch. Difference from measured one could be explained by a bit more complex bunch structure that simple gaussian. From other side, we measure train of pulses, so it could be, that microbunches in train have different width. Spectrum change, as function of phase is shown in figure 16b. BGS for this two spectrums is 10 mm

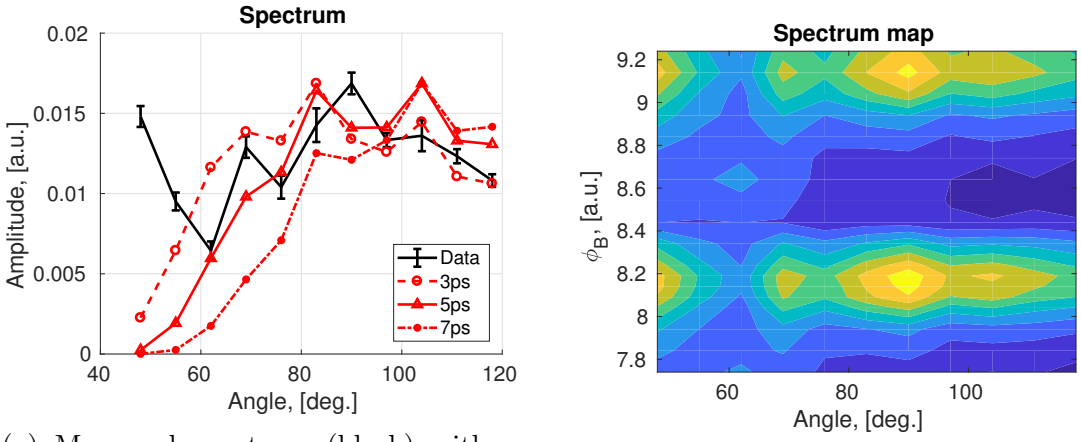

(a) Measured spectrum (black) with predicted spectrum for different bunchlengths (3, 5, 7 ps)

(b) Change of spectrum as function of buncher phase

Figure 16: Experimentally measured spectrums

4.3 Form Factor

We expect to see same Form factor as function of BGS, but from figures 17 we see rapidly changing components as function of BGS. We suppose that it is parasite or

incoherent radiation. But more likely parasite, due to high amplitude.

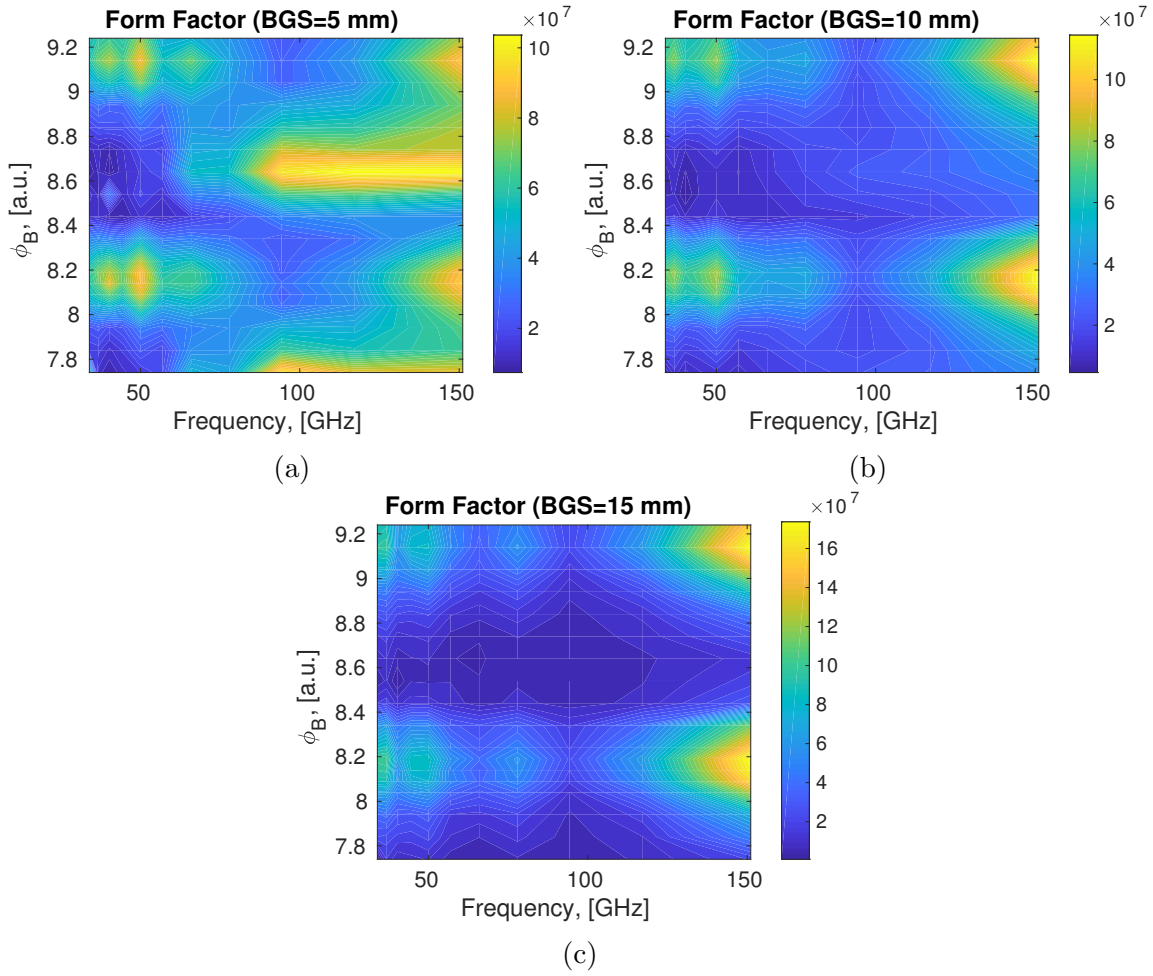

Figure 17: Form factor at different beam-grating separation

Form factor for phase for buncher phase equal $\phi_B = 8.14$ is shown on figure 18a. Its vary in amplitude, but save its shape as function of BGS. Change of amplitude was caused by disagreement of evanescent wave in computation code and experimental data. From figure 18b we see that form factor and so profile on the bunch change with buncher phase.

4.4 Bunch profile reconstruction

We apply spectrum recovery procedure as was mention in [2]. We use most optimized bunch form-factror ($\phi_B = 8.14$) for normalization of the the form-factors of others bunches. In our reconstruction we didn't take into account first two points in spectrum.

The result of spectrum recovery for several bunch phases is presented on figure 19. Next step is profile recovery. At this point we use Hilbert method of phase recovery,

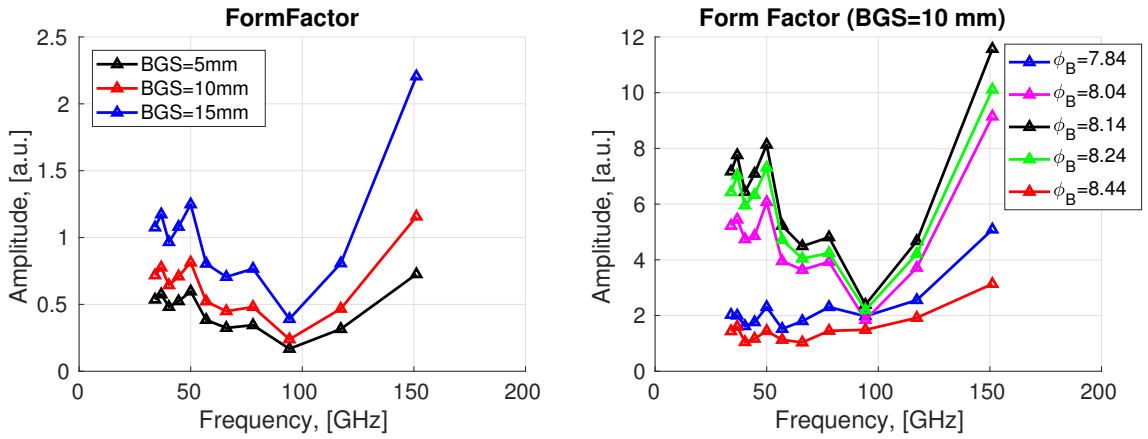

(a) Form factor at different beam-grating separation for certain buncher phase

(b) Form factor at different buncher phase for certain beam-grating separation

Figure 18

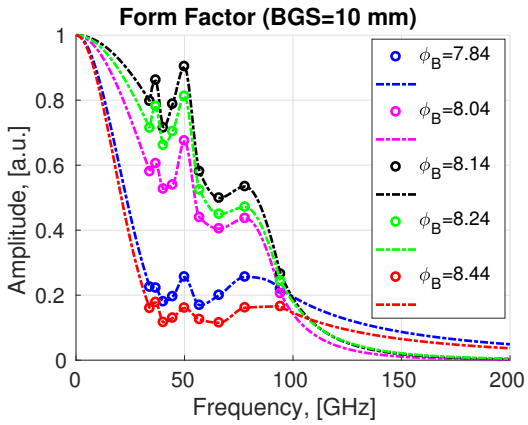

Figure 19: Reconstructed form factor from measured spectrum.

as it gives the best result [2]. After we made inverse Fourier transform. Result of reconstruction is presented on figure 20 and 21b.

Change of bunch width at 10%, 50% and 90% of maximum is presented on figure 21a. For phase $\phi_B = 8.14$, we have: FW0.1M=2.7ps, FWHM=6.8ps, FW0.9M=11.1ps.

To check the correctness of the procedure we calculate spectrum with this achieved profile and compare it with measured (see figure 22a). The difference shows that in spectrum we have component which exponentially decrease with angle. This is background of our measurement. Nature of this component is under investigation.

Also, to estimate error of profile reconstruction, we introduce noise in spectrum in calculated error bounds and reconstruct profile (set of 100 profiles, see fig. 22b). We get that $FWHM = 6.8 \pm 0.3ps$ within 3 sigma change of the spectrum components.

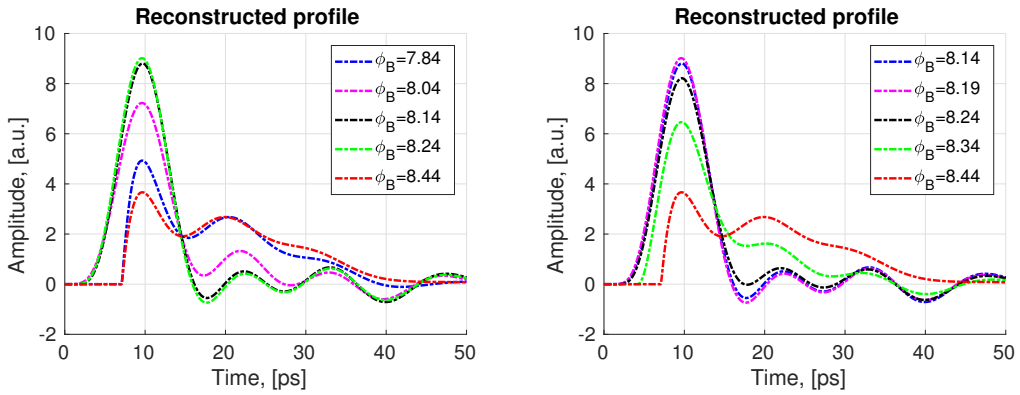

Figure 20: Reconstructed beam profiles for different buncher phase

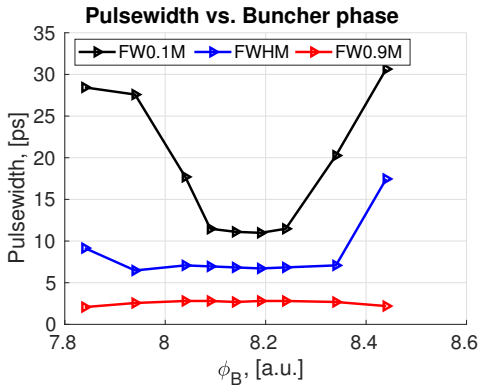

(a) Change of beam width at different level of maximum for different buncher phases

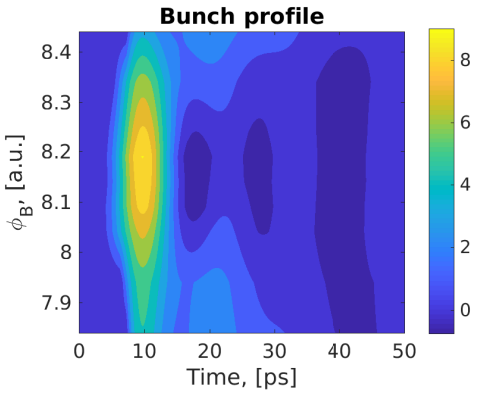

(b) Evolution of bunch profile as function of buncher phase

Figure 21

5 Buncher power

Same study was done for spectrum's as function of buncher power. We made same procedure of data extraction, but get other behaviour of coefficient change (see 23). Coefficient stay constant until reaching the bunch power equal 1.2. Peak of evanescent wavelengthes was caused by bad fitting of data curve (as result of noisy data).

In particular case (see 24) we see small increase in amplitude and alsomost constant change in evanescent wavelength. As "theoretical" we suppose increase in bunch energy from 38.2 MeV for 1.2 [a.u.] of buncher power to 44.2 MeV at maximum buncher power. In this range of energies, evanescent wavelength almost not change (small decrease), as shown on figure 24a by solid line. In general evanescent wavelength is in the previous trend (see fig. 25)

Spectrum change as function of buncher power is presented on figure 26a and 26b.

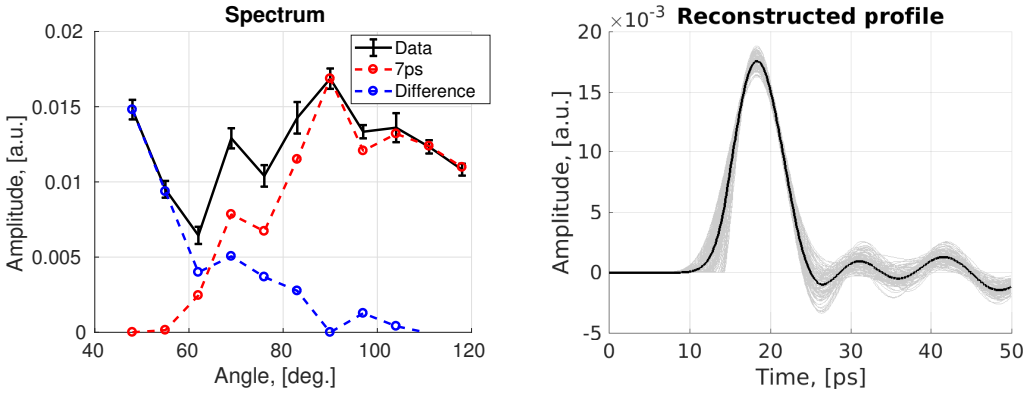

(a) Comparison of measured spectrum (black), calculated from reconstructed profile (red) and difference (blue)

(b) Mean (black) of reconstructed profiles (gray) with introduced noise in form factor

Figure 22

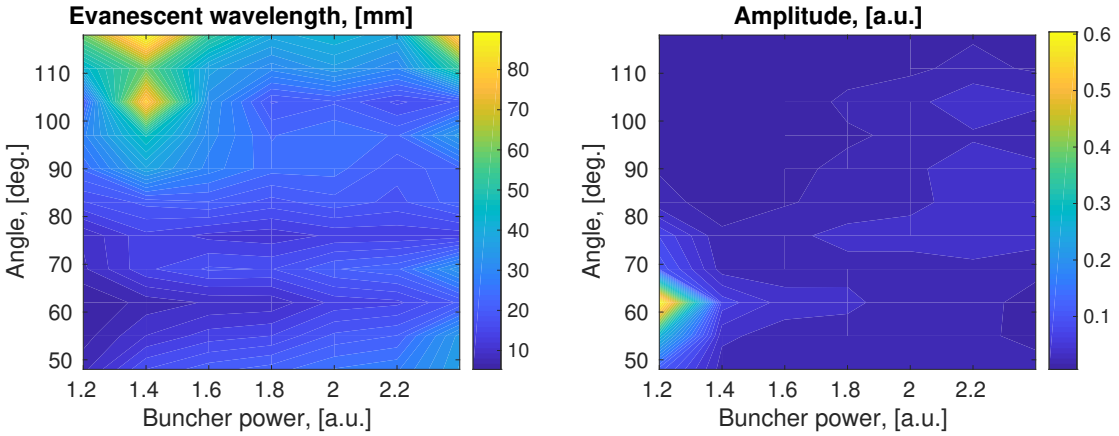

(a) Change of evanescence wavelength as function of buncher power

(b) Change of signal amplitude as function of buncher power

Figure 23

With low power of buncher, Its impossible to form good bunch for further acceleration.

On figure 27a presented interpolated and extrapolated Form factor. FWHM and FW0.1M not really depend from buncher power, but FW0.9M increase almost twice with decrease of buncher power. That indicate on bad compression of tail of the bunch.

Profile evolution is presented on figure 28

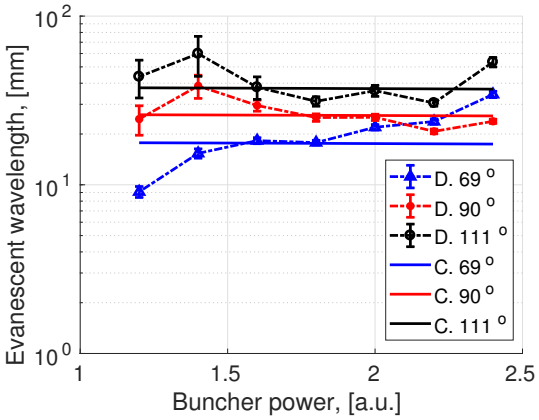

(a) Change of evanescence wavelength as function of buncher power

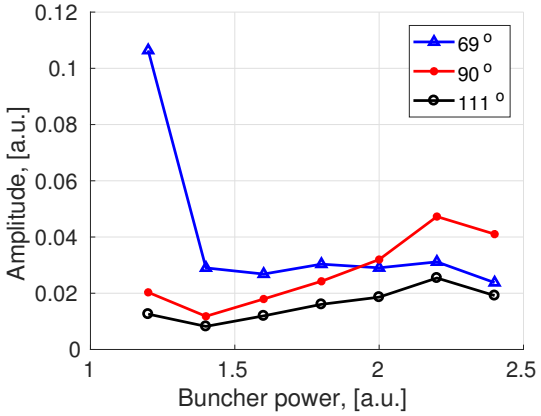

(b) Change of signal amplitude as function of buncher power

Figure 24

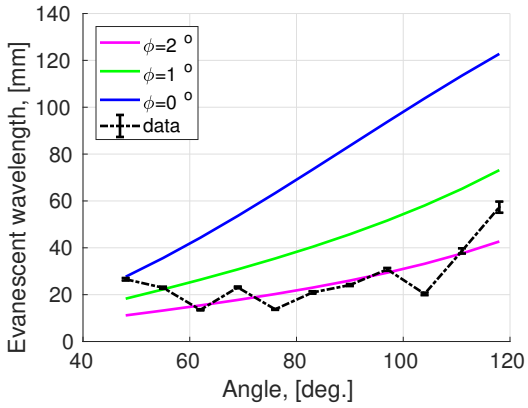

Figure 25: Weighted mean evanescence wavelengths as function of observation angle

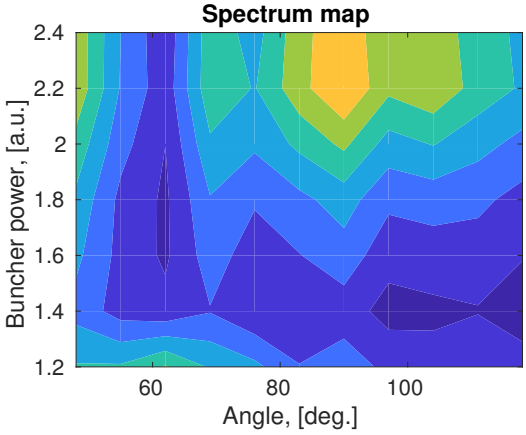

(a) Change of spectrum with buncher power

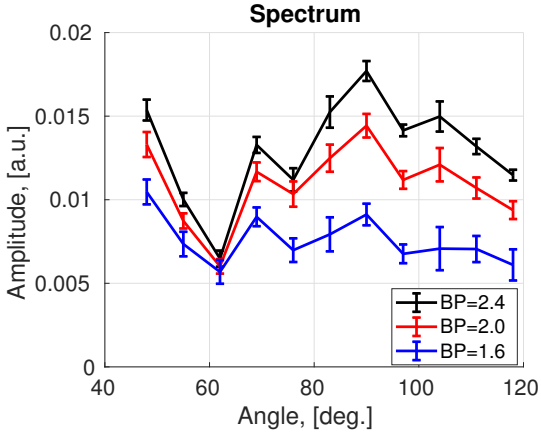

(b) Spectrums for different buncher power

Figure 26

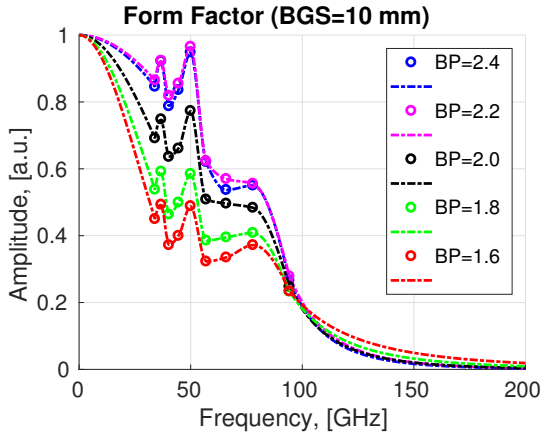

(a) Reconstructed form factor: interpolated and extrapolated

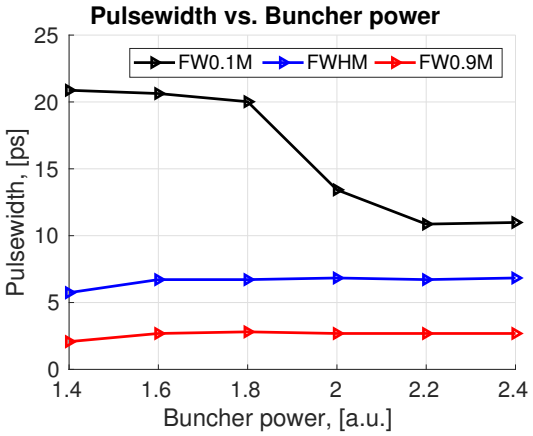

(b) Evolution of bunch width with buncher power

Figure 27

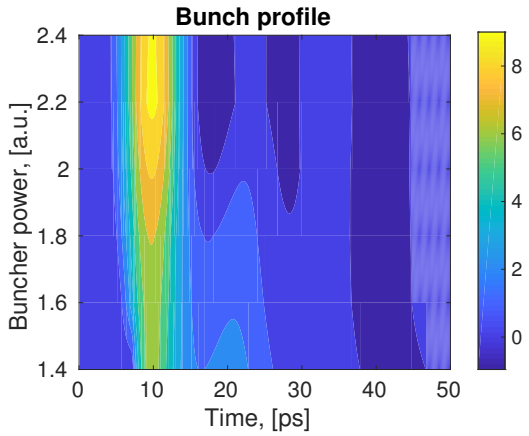

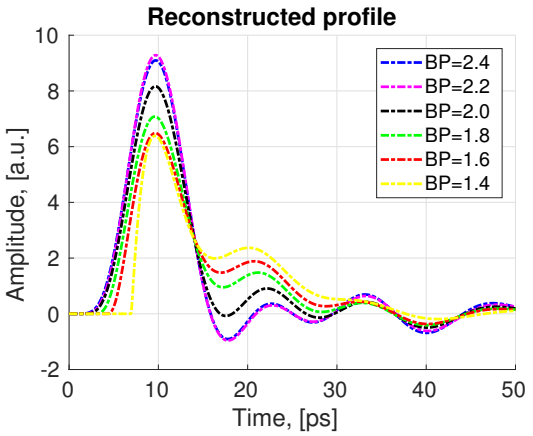

Figure 28: Evolution of bunch profile with buncher power

6 Section phase

Using same method, we obtain follow map for fitting coefficients (see fig. 29a, fig. 29b and fig. 30). Section phase is in units of hundreds from value which we get in control room.

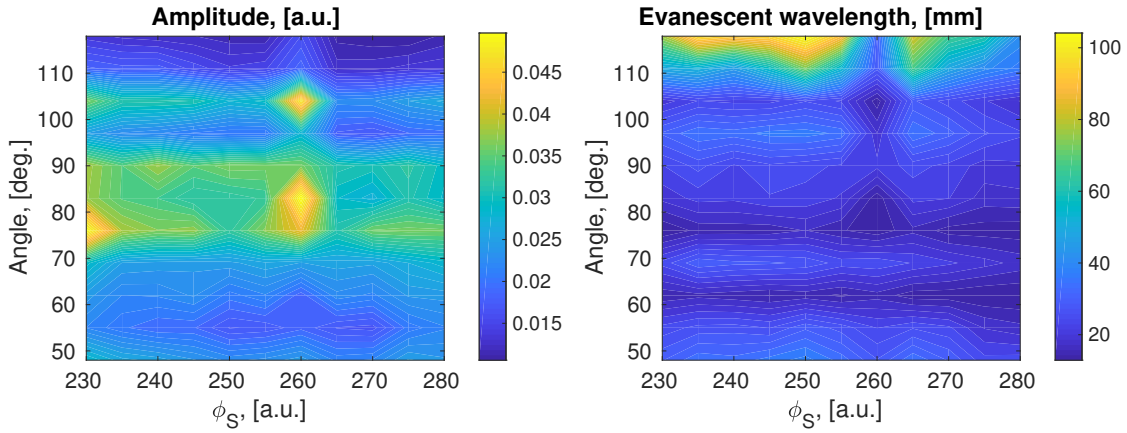

(a) Change of signal amplitude as function of Section phase

(b) Change of evanescent wavelength as function of Section phase

Figure 29

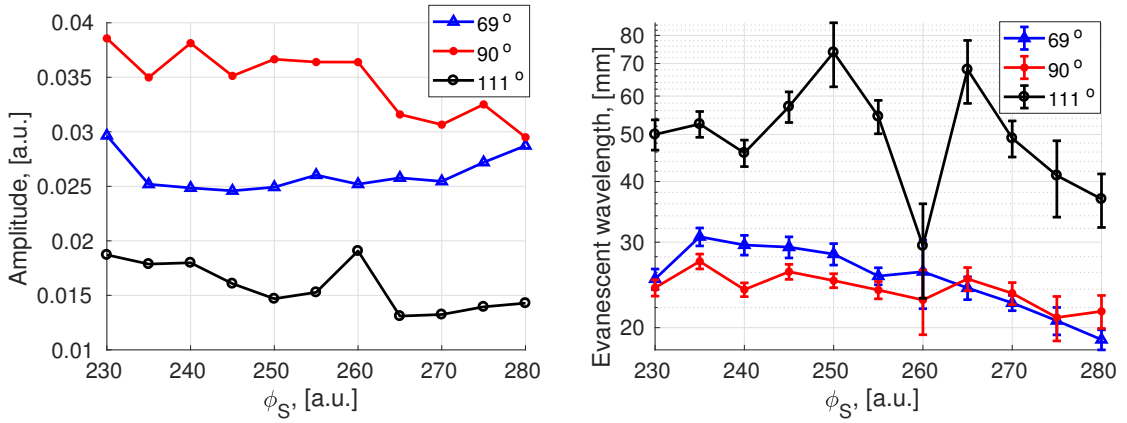

(a) Change of signal amplitude as function of Section phase

(b) Change of evanescent wavelength as function of Section phase

Figure 30

In this calculation was negleged change of SEY, but even with this assumption we see that profile didnt change a lot, as we espect. Second conclusion:

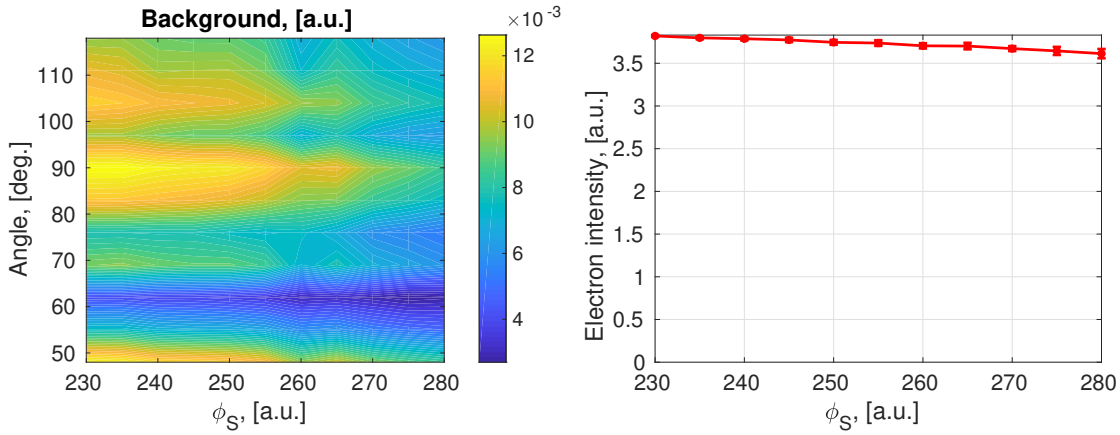

(a) Background of fit

(b) Change of electron intensity

Figure 31

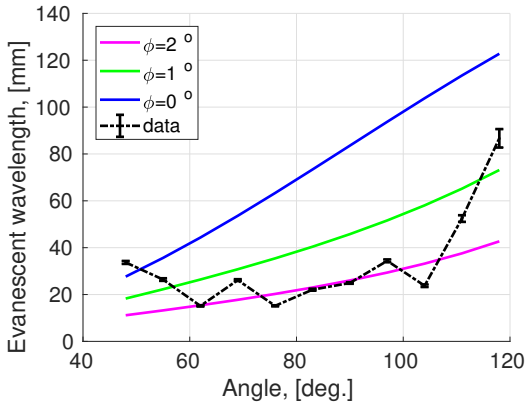

Figure 32: Weighted mean evanescence wavelengths as function of observation angle

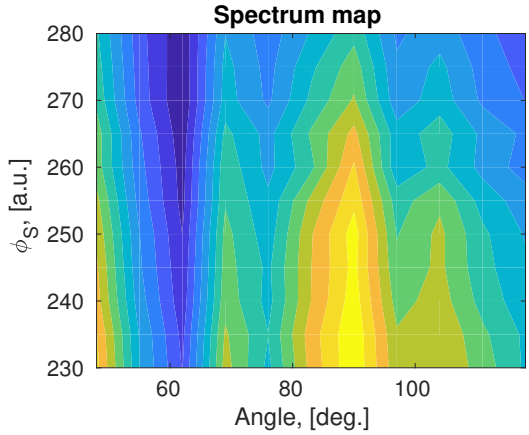

(a) Change of spectrum with section phase

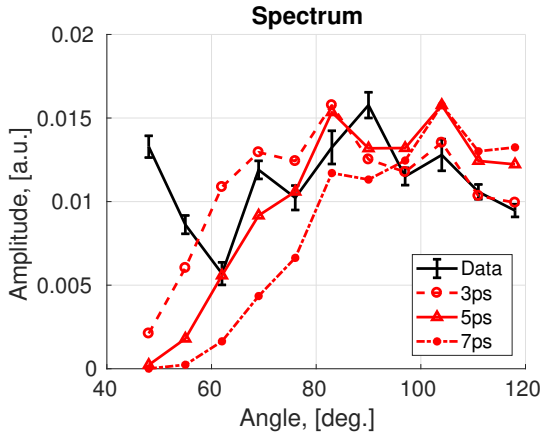

(b) Measured spectrum with prediction (gfw.m)

Figure 33

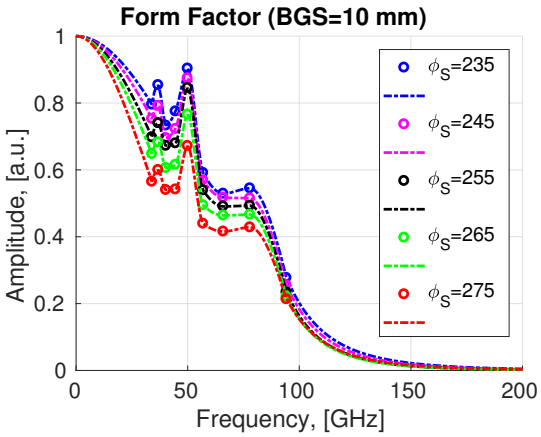

(a) reconstructed form factor

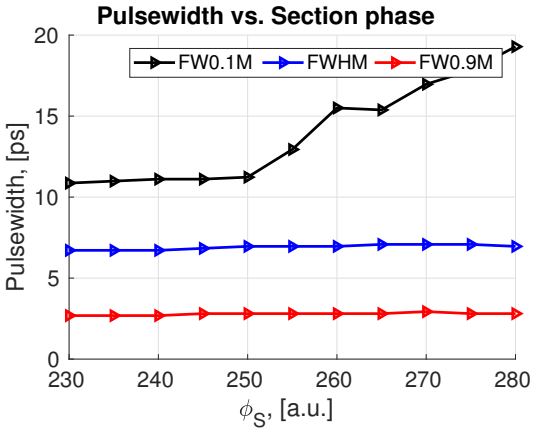

(b) Evolution of bunch width with section phase

Figure 34

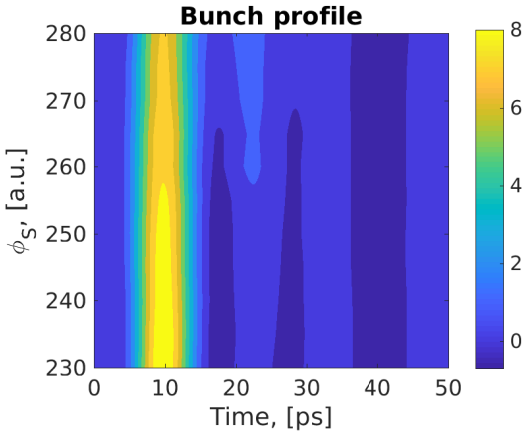

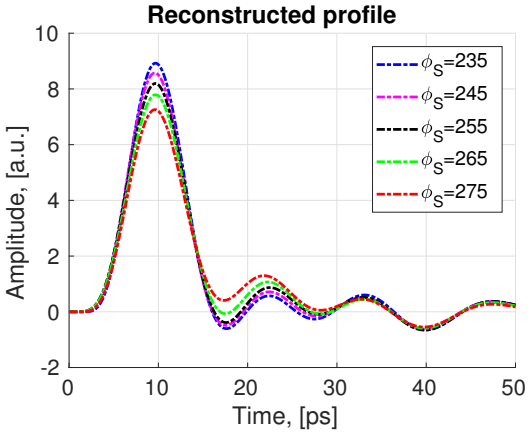

Figure 35: Evolution of bunch profile with section phase

Primary comparison with ASTRA simulation

In [**?**] was described ASTRA model of CLIO accelerator. In this section we compare our simulation with experimental results.

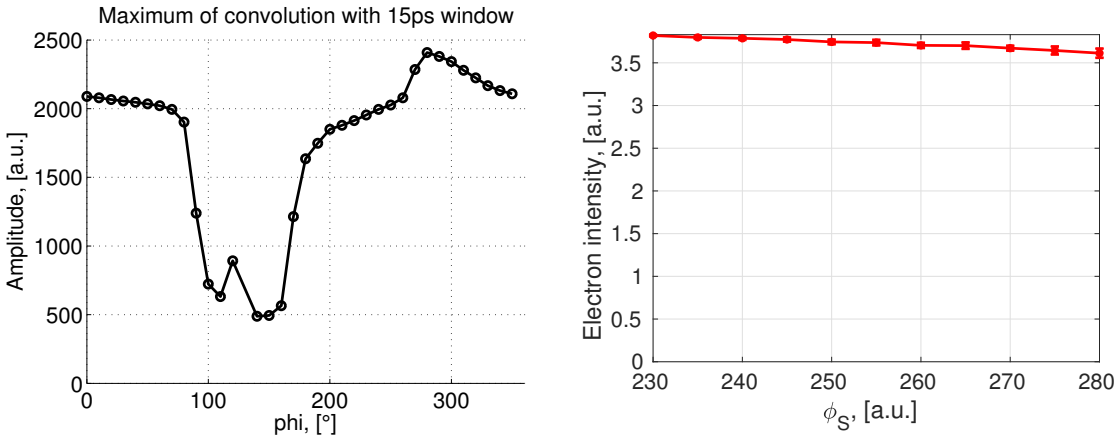

(a) Astra simulations

(b) Experimental measurements

Figure 36: Bunch intensity

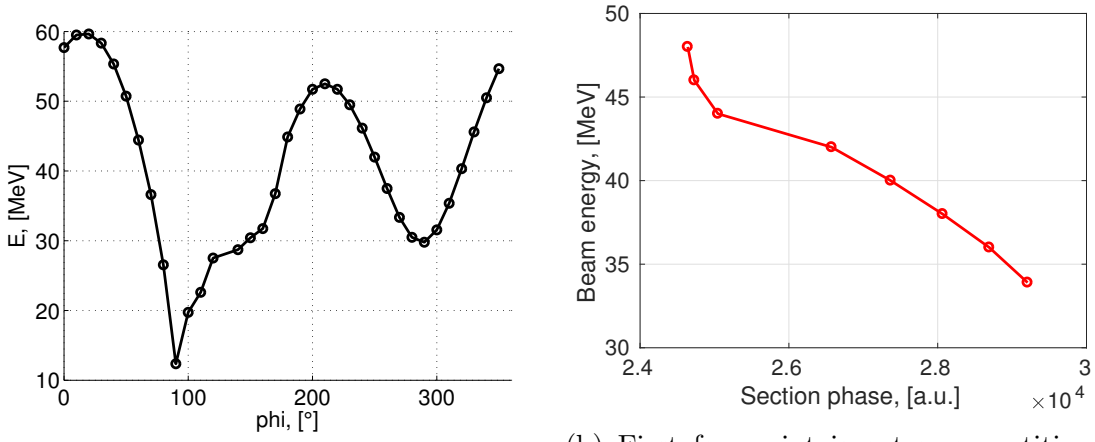

(a) Astra simulations

(b) First few point is extreme contition for accelerator

Figure 37: Bunch energy

At this point we could conclude, that we are at the beginning of phase diapason, because:

- Electron intencity not depend a lot from section phase
- We have similar behaviour of beam energy from section phase
- FWHM and FW0.1M also have similar behaviour in this region

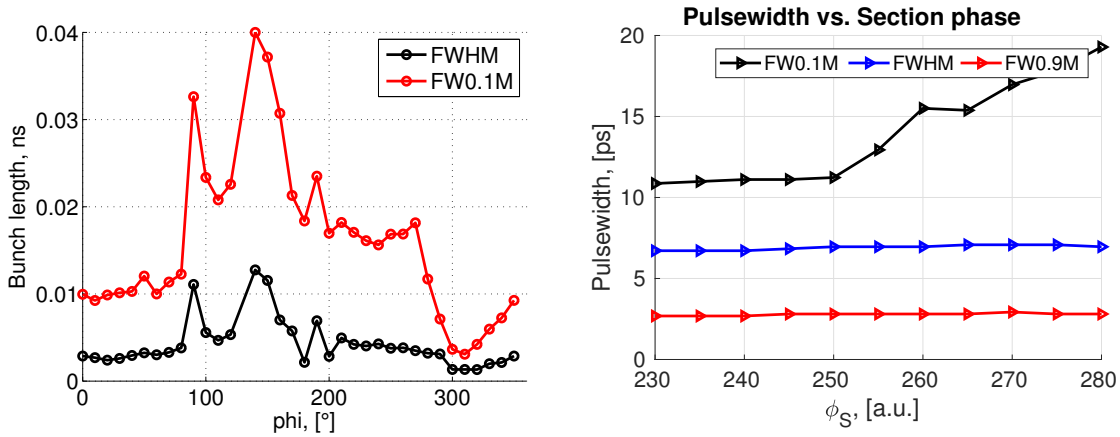

(a) Astra simulations

(b) Experimental results

Figure 38: Bunch width

7 Short results for 3 mm pitch grating

Using same algorithm we analyse data wiht 3 mm grating. Results will commended in case of need.

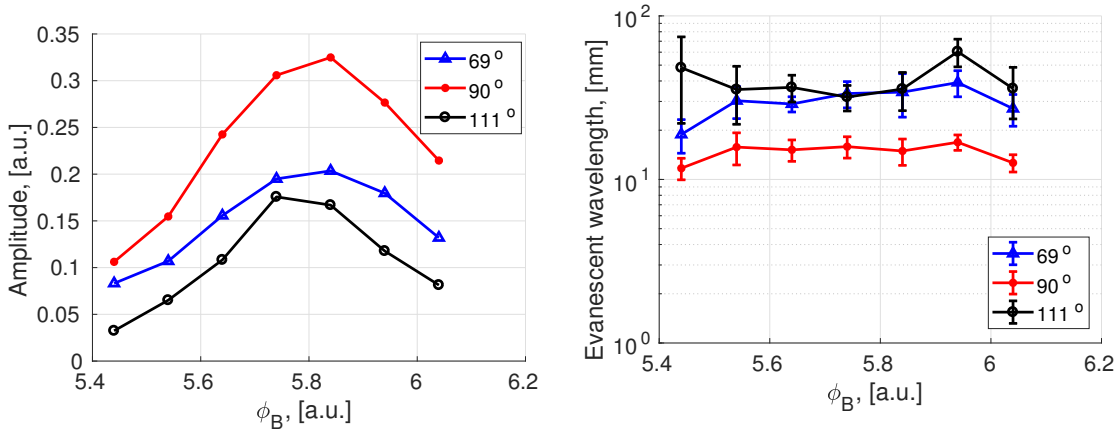

(a) Change of amplitude with buncher phase

(b) Change of evanescent wavelength with buncher phase

Figure 39

Important point to compare form factor to both grating. As measurements was done at different days with different alignment, their require different normalization. We choose this coefficients for one case (best bunch) and compare Form factor for other phases with same coefficients (see fig. 43)

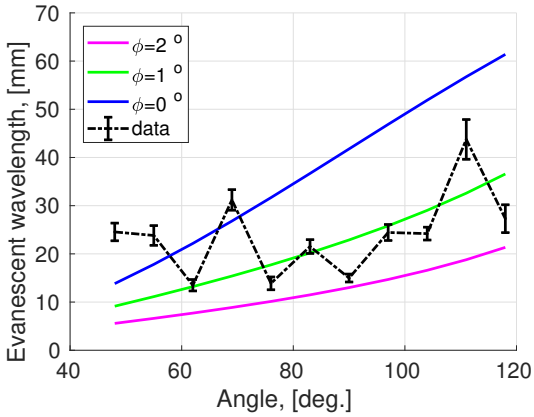

Figure 40: weighted mean evanescent wavelength

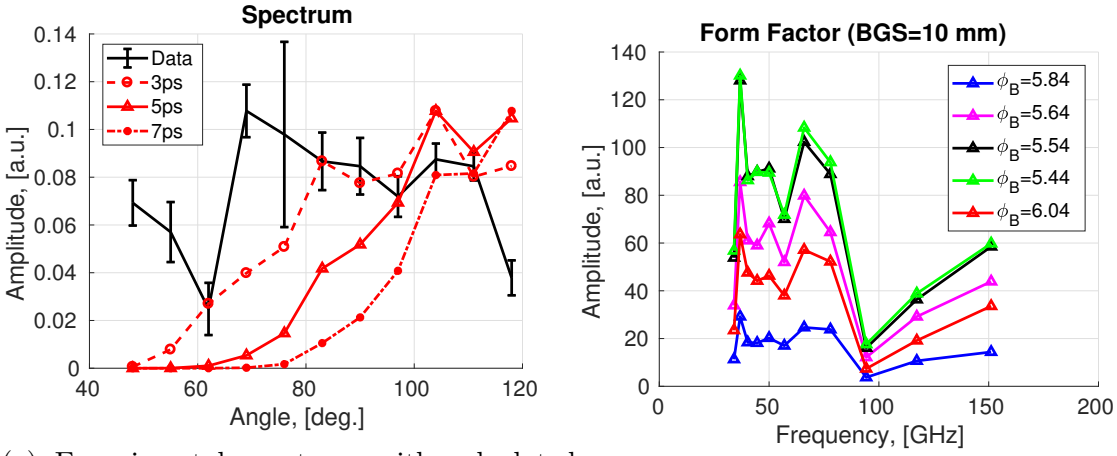

(a) Experimental spectrum with calculated with gfw

(b) Form factor for different buncher phase

Figure 41

8 Conclusion

With current setup we could measure radiative phenomenas which have similar behavior with Smith-Purcell radiation. In assumption, that we measure coherent SPR, we could estimate bunch lengths for certain parameters of CLIO accelerator.

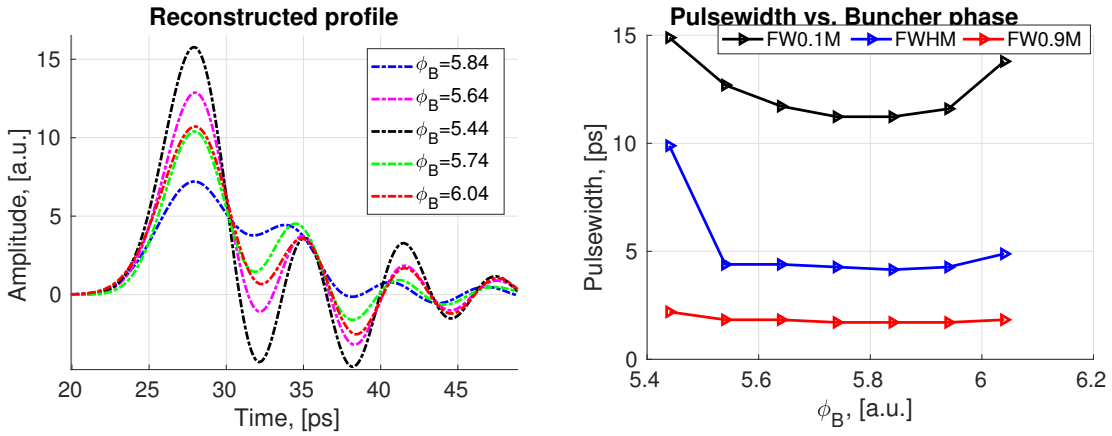

(a) Reconstructed profiles with 3 mm grating for different buncher phase

(b) Change on bunch width with buncher phase

Figure 42

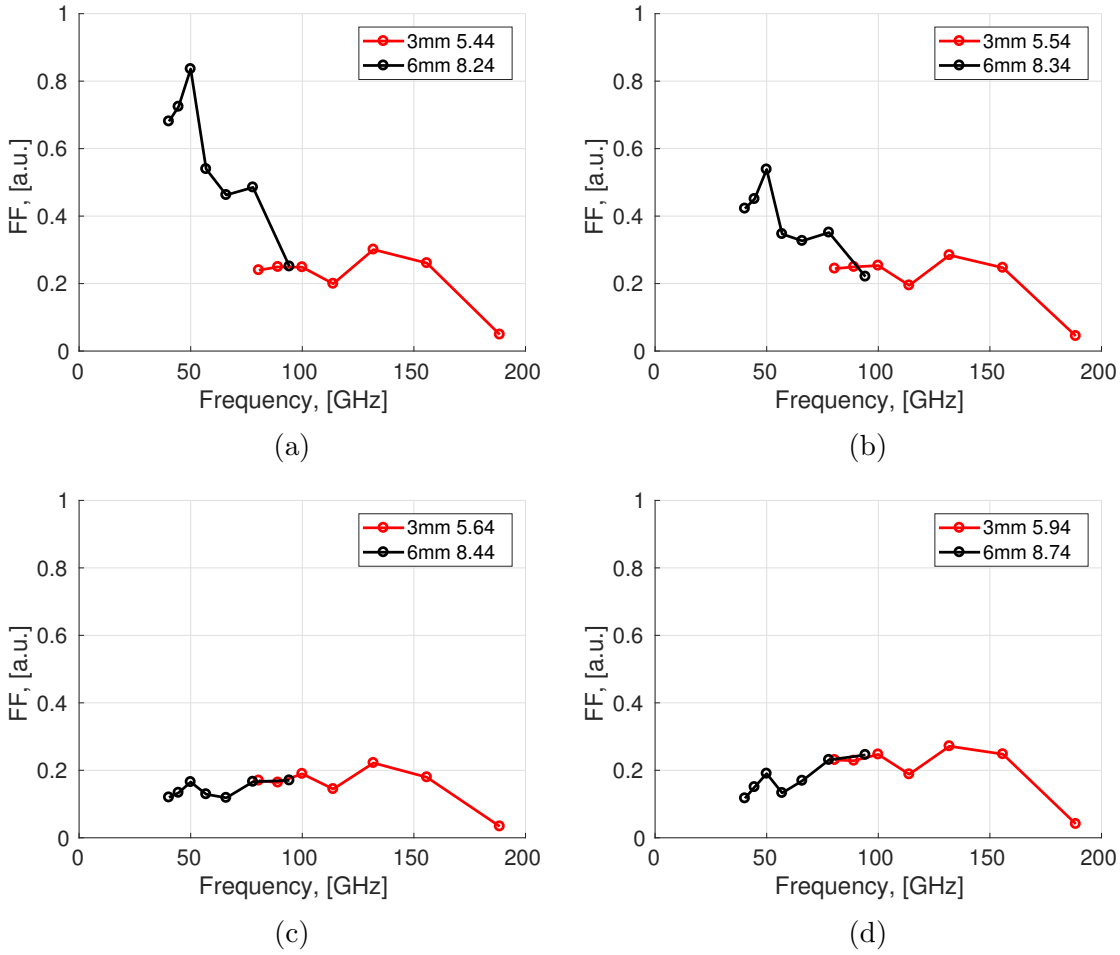

Figure 43: Form factor for two gratings (3 mm in red and 6 mm in black). Step in buncher phase is same.

9 Appendix

9.1 Position calibration

One step of motor equal 7.94 nm. For current calibration we use motor steps as reference.

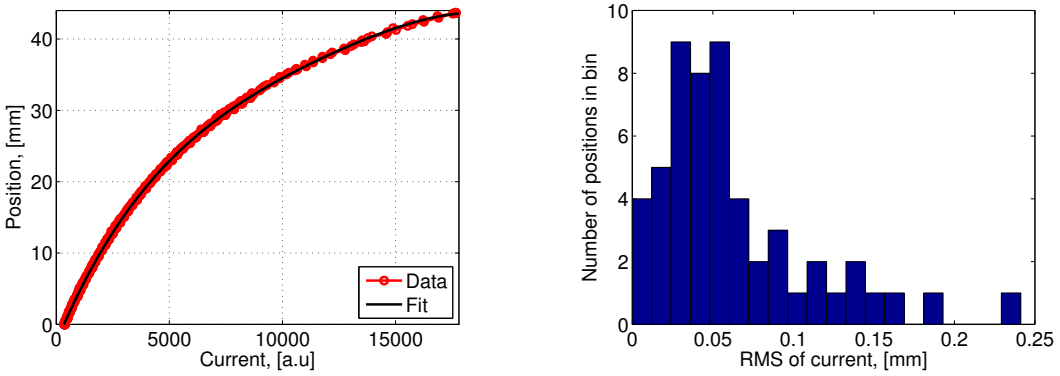

(a) Position calibration

(b) RMS histo for current measuremets

Figure 44: Position calibration

With polynomial fit we get:

$$f(x) = -8.374e-11 * x^4 + 4.053e-06 * x^3 + -0.08082 * x^2 + 952.6 * x - 3.141e+05$$

As current measurements are variable in time for same position. By taking fit of this data with gaussian, we find peak at the **0.04 mm**, which define precision of position determination with potentiometer.

9.2 Correction of defocusing

If grating is in focus of OAP mirrors, all detectors see centers of the grating (see fig. 45a). Turned by defined angle, mirror saw bigger grating surface (represented by red ellipse on the schema). If grating is small, ellipse could be bigger than grating. Cross-section of ellipse and rectangular define this correction.

Except this, grating could move along X direction (closer and far from the beam). Depending where grating is, its also define correction on defocussing.

Script Grating_correction.m

9.3 Mirror acceptance

Cross-section of two circles (detector and focus point of abbe diffraction limit).

Focus spot is circle with radius defined by Abbe difraction limit. Detector diameter is fixed and equal 2 mm and supposed to be exactly in focus of 25mm with 50.8 focus length OAP mirror.

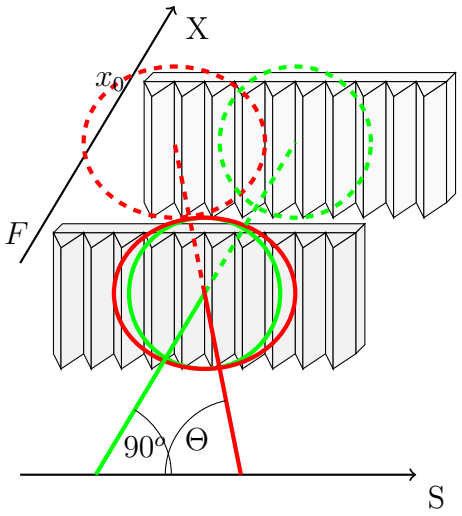

(a) Correction of defocusing

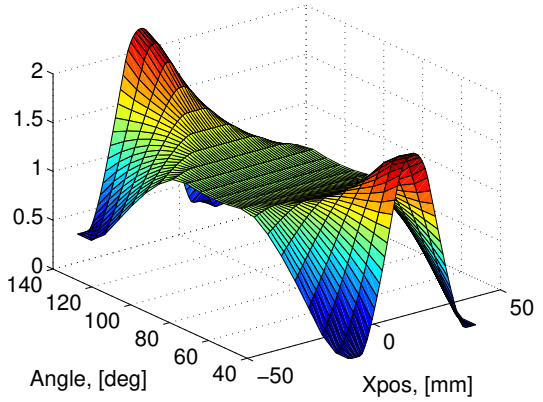

(b) Correction on defocusing for 25 mm spherical mirror and 20x40 mm grating size as function as grating position

Also was taken into account, that frequency of SPR depent from observation angle, so at different angle we have different spot size. Script OverlapCorrections.m

9.4 Beam size

This experiment was done by cutting with 3 mm grating beam and measuring electron intensity. Grating tooth height should be taken into account! Script Beam_size.m

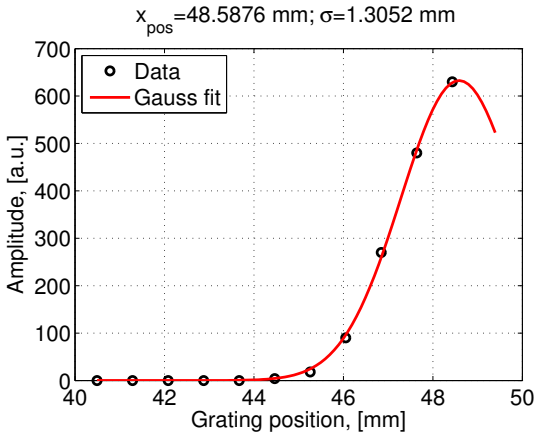

Figure 46: Transverse beam size at CLIO

9.5 Section phase/energy

Calibration of Section phase vs. Energy. Script PhaseEnergy.m

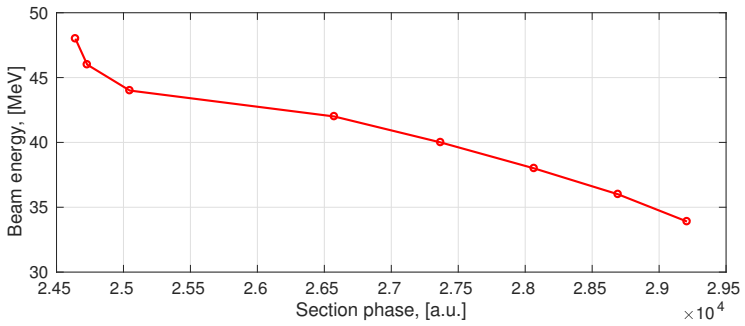

Figure 47: Section phase vs. beam energy

10 Notes

Understand or improve:

- Simple min of electron signal COULD be source of problems due to inductive character of the line. So measured in this way signal could be over-evaluated.
- Normalize on Electron intensity or square of Electron intensity??!!!
- Nature of background and the methods of background rejection require further investigation
- Understand change of EW with parametrs. Evaluate change of γ with buncher phase. Behaviour of evanescent wavelength require further experimental checks and advanced correction (acceptance angle ...) in theory!
- SEY for 44.2 MeV in section phase
- Is current setup is sufficient to study change of spectrum as function of bunch energy.
- Should be developed advanced model of CLIO accelerator. Results of SPR measurement should be compared with ASTRA model!

In experiment:

- Install THz filters to reduce noise.
- Absolute detector calibration. A lot depend on Spectrum normalization. Now its completely arbitrary choise.

In gfw code:

- Energy spread should be taken into account in gfw calculation
- Experimental corrections: Calculate EW with this correction on beam spot. Also decay in quartz window (+ reflection), and air

- Take into account in gfw code different angle of observation (ϕ). Take into account correction on aberration (ellips+circle)

References

[1] J. Walsh J. H. Brownell and G. Doucas. Spontaneous smith-purcell radiation described through induced surface currents. *Phys. Rev*, 1998.

[2] N. Delerue et al. Study of phase reconstruction techniques applied to smith-purcell radiation measurements. In *IPAC17*.